Study of impedance model and water transport behavior of modified solvent-free epoxy anti-corrosion coating by EIS II

Rui Ding, Wei-wei Cong, Jian-ming Jiang, Tai-jiang Gui

Abstract This work studied the evolution of an impedance model of 60 μm modified solvent-free epoxy anti-corrosion coating on a Q235 steel surface in 3.5% NaCl solution using electrochemical impedance spectroscopy. The electrochemical process of the system was divided into five stages. During the early stage of immersion, water absorption occurred mainly at the coating, coating resistance decreased, and coating impedance deviated from purely capacitive characteristics. The corrosion reaction started after water permeated into the metal/coating interface. During the mid-immersion stage, the electrochemical reaction at the coating/metal interface was controlled by semi-infinite diffusion of corrosion products due to the barrier effect of the coating. The types of corrosion product diffusion gradually became finite layer diffusion and barrier layer diffusion with the clogging of coating pores. Logarithm of coating capacitance and the square root of time showed a linear relationship in the early immersion stage, which was a typical characteristic of Fick's diffusion. Afterwards, increase in the coating capacitance slowed down, and a non-Fickian diffusion process occurred, which presented the two-stage absorption characteristics. Water diffusion coefficient in coating was calculated to be 2.95×10^{-10} cm^2/s, while volume fraction and total water absorption at saturation of coating were 2.3% and 185 μg, respectively, indicating good water resistance and protective properties of the coating. The water kinetic equation in the coating which can reflect the whole Fick diffusion process of water and containing time and location variables was obtained via the Fick diffusion equation and three-dimensional images of water distribution in the coating were drawn by transforming the dynamic equation into programs.

Introduction

Oceans are very harsh corrosive environments, so ships and marine engineering structures are subject to severe corrosion in the marine environment. Anti-corrosion coatings are a widely used anti-corrosion technique owing to their high economical efficiency, good protective effect, and simple fabricating process. Because of the widespread use of anti-corrosion coatings, research on coating failure processes, prediction of coating service life, and detection of coating status have been popular research topics. Meanwhile, many research approaches have been developed as well. Among them, electrochemical means, particularly electrochemical impedance spectroscopy, is the most widely used method. Electrochemical impedance spectroscopy technique applies small-amplitude sinusoidal alternating perturbation signal to the researching system and collects the system's response signal.[1] As the applied perturbation signal is very small, which does not cause any irreversible impact on the properties of sample system, electrical parameters related to the performance of the coating/metal system and coating failure process can be measured in situ, such as capacitance and resistance of coating, double layer capacitance of coating/metal interface, and charge transfer resistance.[2] With the above advantages, electrochemical impedance spectroscopy has become a major approach for studying the corrosion behavior of organic coating/metal systems.

The protective effect of organic coatings lies first in their barrier effect against corrosive particles, so permeation resistance is an important measure of the quality and anti-corrosion efficiency of coatings.[3] In various environments in which coatings are used, water

R. Ding (✉), W. Cong, J. Jiang, T. Gui
Marine Chemical Research Institute, State Key Laboratory of Marine Coatings, Qingdao 266071, China
e-mail: dmoyuyang@foxmail.com

and oxygen are the two most common corrosive particles which can penetrate into the coatings by diffusion.[4] Numerous studies have confirmed that water plays a major role in the corrosion process of metals.[5–8] There are gravimetric methods and capacitance methods for studying water transport in organic coatings. After extensive experimental studies, it has been found that the capacitance method is more advantageous than the gravimetric method in the study of water transport in coatings and polymer films that are only a few microns thick. In addition, the capacitance method is faster and more reliable, which allows coating properties such as diffusion coefficient and solubility of water or saturated water absorption and dielectric constant to be obtained.[9,10]

In the Chinese domestic market, a variety of high-performance epoxy coatings, polyurethane coatings, acrylic coatings, and inorganic zinc coatings have been developed aside from the traditional oil-based coatings, phenolic resin coatings, and alkyd resin coatings. Among them, epoxy coatings are the most widely used type of coatings in the shipbuilding industry, and account for over 85% of the shipbuilding market.[11] However, most of these coatings contain large amounts of organic solvents, which are not in line with the trend of green and environmental protection. Therefore, in this work, MYF coating (modified epoxy anti-corrosion coating) in Chinese Pinyin, developed independently by the China Marine Chemical Research Institute was studied for the evolution of electrochemical impedance response, water transport behavior, etc.

In previous work, the authors studied the impedance model evolution and water transport behavior of 30 μm MYF coating, which showed that the electrochemical impedance evolution of the coating/metal system was divided into five stages: initial water absorption, occurrence of corrosion, Warburg diffusion control, stripping of coating, and coating failure.[12] The water absorbing process of the coating followed Fick's law, which reached water saturation after immersion for about 25–30 h. Water diffusion coefficient in the coating was calculated to be 8.23×10^{-11} cm^2/s. Volume fraction and total water absorption of coating at water saturation were 3.5% and 105 μg/cm^2, respectively, presenting good water resistance and barrier properties. This study derived the diffusion kinetic model before water contact with the coating/metal interface, and calculated the time at which corrosion reaction started at the coating/metal interface to be about 3.31 h after immersion.

This paper will continue to study the impedance model and water transport behavior of 60 μm MYF coatings. The 60-μm coatings exhibited completely different impedance evolutions from the 30-μm coating, since the early-mid period of immersion, and presented very different water transfer characteristics as well.

Experimental methods and materials

Experimental materials and preparation of specimens

Components of Q235 steel used in the experiments are shown in Table 1. Samples were cut into 50 mm × 50 mm × 3 mm sheets, sand-papered, and washed with deionized water. The coating used in the experiments was MYF coating from the Marine Chemical Research Institute, while curing agent was the modified polyamine epoxy curing agent. Thirty and 60 μm thick coatings were prepared in the experiments, which were sealed and stored after complete curing. In previous work, 30 μm coating was studied.[12] In this paper, 60 μm coating will be discussed. Figure 1 shows a three-dimensional map of the coating thickness ranging from about 55 to 63 μm as measured by the thickness gage produced by Phoenix Contact GmbH & Co. KG.

EIS measurement

The experiments measured the impedance response of MYF coating/Q235 steel system in 3.5% NaCl solution using a three-electrode system. Coated steel was used as the working electrode, saturated calomel electrode served as the reference electrode, and platinum electrode served as the auxiliary electrode. Electrochemical workstation used was Princeton's PAR 2273, while measuring software was PowerSuite electrochemical test system. During the measurement, sinusoidal AC potential disturbance 10 mV (voltage peak value) with respect to the open circuit potential was applied to the coated steel system, and the measurement frequency range was 100 kHz–10 mHz. All experiments were performed at room temperature. Experimental data were analyzed using ZSimpWin Version 3.00 software.

Results and discussion

Evolution of impedance and equivalent circuit model

In the following, impedance evolution will be discussed using the 60-μm coating as an example. During the

Table 1: Components of Q235 steel

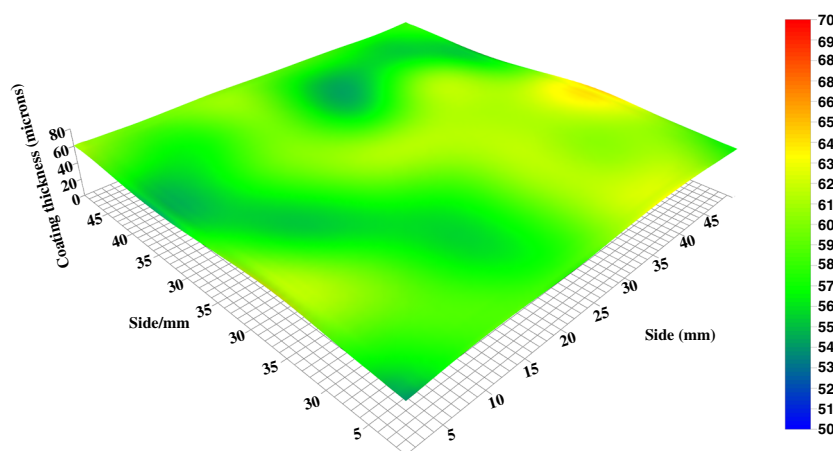| Components	C	Mn	Si	S	P	Fe
Wt%	0.14–0.22	0.30–0.65	0.30	0.05	0.045	Margin

Fig. 1: Three-dimensional map of the coating thickness

early stage of immersion, the coating exhibited high impedance characteristics; the impedance complex plane of coating/metal electrode system was manifested as a straight line almost perpendicular to the real axis; and in the Bode diagram, the impedance modulus $|Z|$ showed a linear relationship with a slope of -1 with the logarithm of frequency log f in the entire test frequency range. During this stage, the system could be regarded as a purely capacitive element.

Initial water absorption

After soaking for a short time (20 min–5 h, as shown in Fig. 2), resistance behavior began to occur at the low-frequency region because the impedance spectra of coating/metal system began to deviate gradually from purely capacitive behavior due to coating water absorption. The Nyquist plot presented a circular arc with a large radius which decreased with immersion time, and the phase angle showed a decreasing trend in the low-frequency region with shortening immersion time, indicating reduced coating resistance and increased capacitance as a result of coating water absorption (Fig. 3).

During this stage, the coating was equivalently a resistor with a high impedance connected in parallel with a capacitor element with a low capacitance. Each electrical parameter of coating/metal system at this stage could be obtained by fitting impedance data using equivalent circuit model A, where R_s was the solution resistance, Q_c was the coating capacitance, and R_c was the coating resistance. Due to the non-ideality of the system, capacitive element C was replaced entirely by constant phase angle element Q.[13] The mathematical expression of impedance of equivalent circuit model A has been described in previous work.[12]

Figure 4 shows the fitting results of impedance data after 20-min immersion of coating/metal system using equivalent circuit model A. The equivalent circuit

model A offered good fitting results for all the 20 min–5 h post-immersion impedance data of the system.

Occurrence of corrosion and impeded absorption

Figure 5 shows the impedance spectra after 8 h–8 days immersion of the coating/metal system. The Nyquist plot changed gradually from a circular arc to a semicircle, whose radius decreased over immersion time. Phase angle continued to decrease in the low-frequency region and the peak in the mid-low frequency region was gradually revealed, which moved toward the high-frequency region. This was the second time constant, which indicated the gradual expansion of corrosion reaction area at the coating/metal interface. Impedance modulus decreased at the low-frequency region, and the frequency range of the horizontal section representing resistance characteristics expanded.
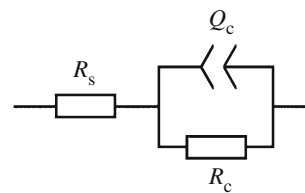
In Fig. 6, the 5 day post-immersion data were fitted as an example using the equivalent circuit A. As can be seen from the figure, although the impedance was a large capacitive arc in appearance, ideal fitting results could not be obtained using the equivalent circuit fitting A, especially in the mid-low frequency region, which could be more intuitively observed from the phase angle diagram.

Since the coating/metal system was immersed for a relatively long period of time in corrosive solution, water and oxygen molecules in the corrosive solution permeated into the coating/metal interface through the coating, causing the electrochemical corrosion reaction of the metal substrate. Therefore, an equivalent circuit model B containing the electrochemical reaction impedance of coating/metal interface was established, where Q_{dl} was the double layer capacitance of substrate metal corrosion reaction, and R_t was the charge transfer resistance of substrate metal corrosion reaction. Water, oxygen, and ions in the solution permeated inside the coating through cracks or micro-
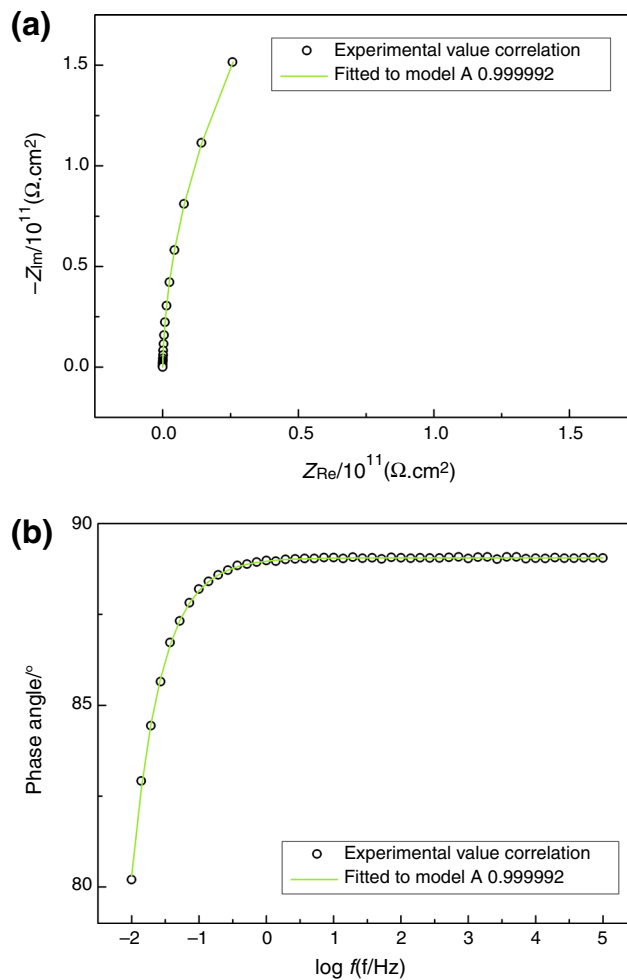
(a)

(b)

(c)
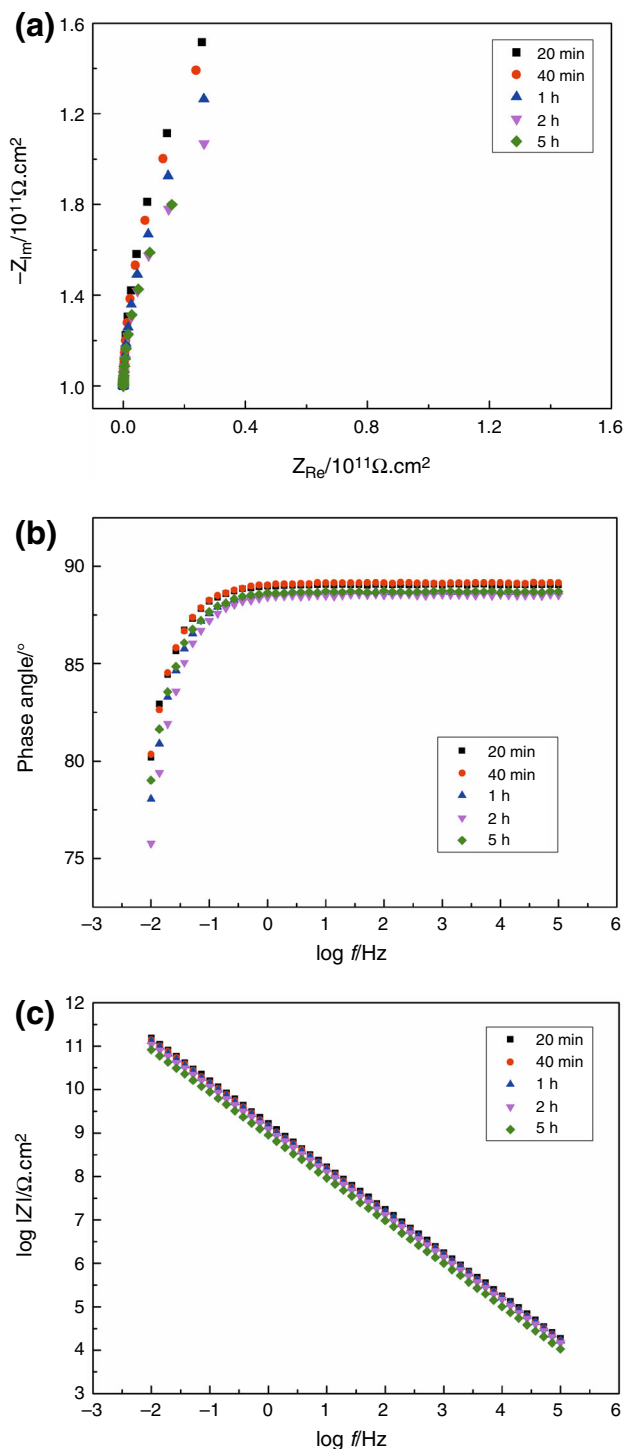
Fig. 2: Impedance spectra of coating/metal system after 20 min–5 h of immersion. (a) Nyquist. (b) Bode-θ. (c) Bode-|Z|

(a)

Fig. 3: Equivalent circuit model A

(a)

(b)

Fig. 4: Impedance spectra and fitting results of coating/ metal system after 20 min of immersion. (a) Nyquist. (b) Bode-θ

pores in the coating. When these corrosive media permeated into the coating/metal interface, current was conducted in the coating mainly through these micropores, and thus coating resistance R_c should be replaced by micro-porous resistance R_{po}. However, the

fitting results using this circuit still deviated from the experimental data in the low and medium frequency regions (Fig. 6). Taking into account that the coating contained flakes like micaceous iron oxides, which would play a barrier role in diffusion within the coating, mass transfer process could become a slow procedure. Thus, an equivalent circuit C was created on the basis of the equivalent circuit B, where Z_w was the Warburg impedance (Figs. 7, 8). Experimental data were fitted very well using this circuit. Nyquist plot contained only one capacitive arc, i.e., one time

(a)

(b)

(c)
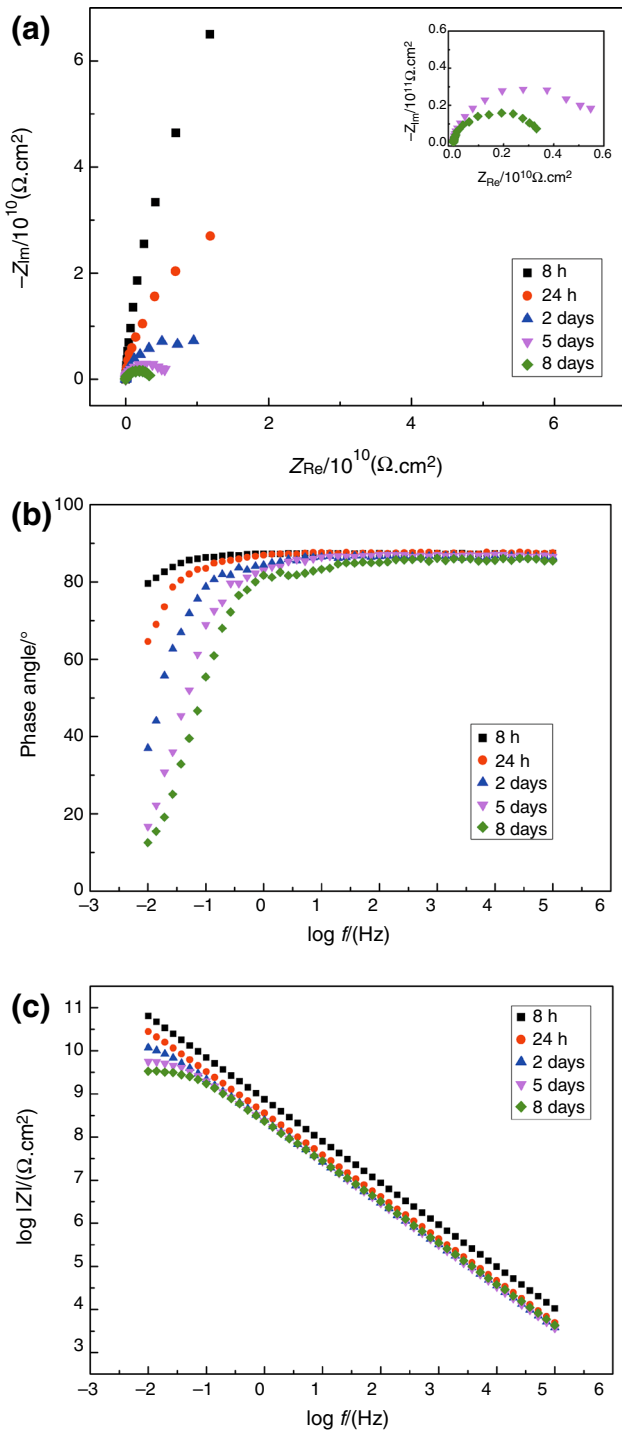
Fig. 5: Impedance spectra of coating/metal system after 8 h–8 days of immersion. (a) Nyquist. (b) Bode-θ. (c) Bode-|Z|

constant. This was because the electrochemical reaction area on the coating/metal interface was relatively small at that stage, resulting in relatively close coating impedance-associated time constant to the electrochemical reaction-associated time constant on the

(a)

(b)
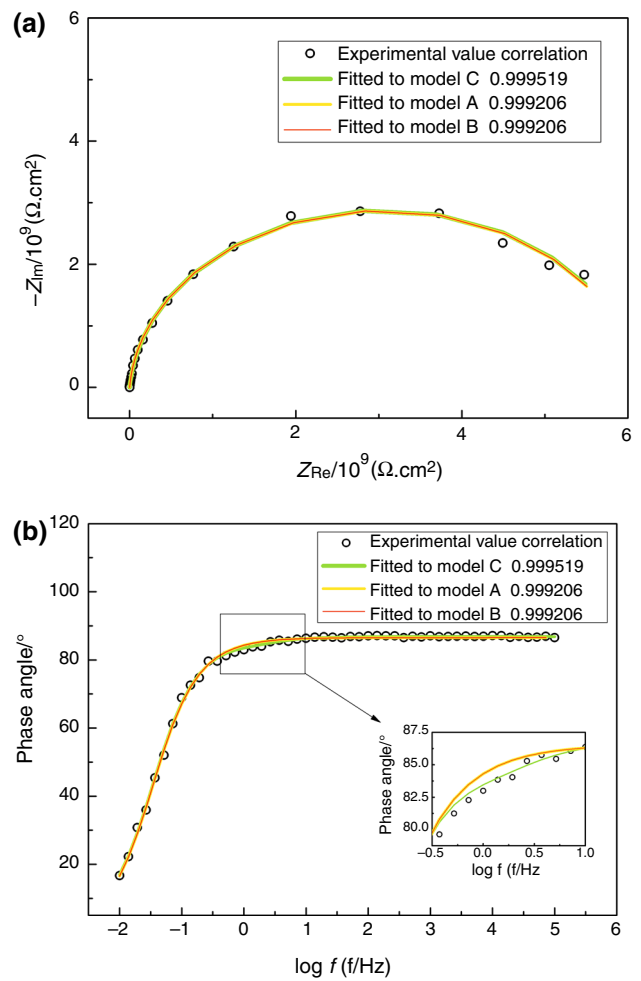
Fig. 6: Impedance spectra and fitting results of coating/ metal system after 5 days of immersion. (a) Nyquist. (b) Bode-θ
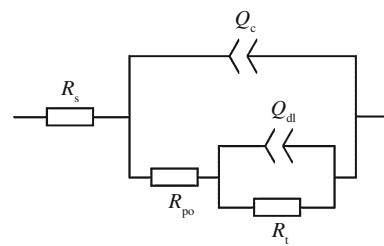
Fig. 7: Equivalent circuit model B
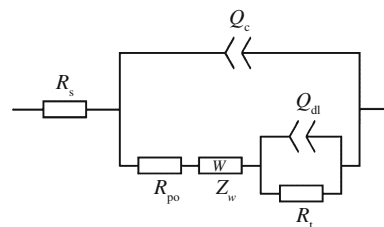
Fig. 8: Equivalent circuit model C

order of magnitude. The two time constants could not be distinguished on the impedance spectra.

Impedance of equivalent circuit model C was

$$Z_C = R_s + \cfrac{1}{Y_{Q_c} + \cfrac{1}{R_{po} + Z_w + \cfrac{1}{Y_{Q_{dl}} + \frac{1}{R_t}}}},$$

where

$$Z_w = \frac{1}{Y_{0,w}}(j\omega)^{-0.5} = \frac{\sqrt{2}}{2}\frac{\omega^{-0.5}}{Y_{0,w}} - j\frac{\sqrt{2}}{2}\frac{\omega^{-0.5}}{Y_{0,w}} = Z_w' - jZ_w''.$$

By separating the real part and imaginary parts, impedance Z_C could be

$$Z_C = R_s + \frac{M_C' N_C' + M_C'' N_C''}{M_C'^2 + M_C''^2} - j\frac{N_C' M_C'' - N_C'' M_C'}{M_C'^2 + M_C''^2},$$

where

$$\begin{aligned} M_C' = {} & 1 + R_t Y_{Q_{dl}}' \\ & + Y_{Q_c}'\left[\left(R_t Y_{Q_{dl}}' + 1\right)\left(R_{po} + Z_w'\right) + R_t\left(Y_{Q_{dl}}'' Z_w'' + 1\right)\right] \\ & + Y_{Q_c}''\left[\left(R_t Y_{Q_{dl}}' + 1\right)Z_w'' - R_t Y_{Q_{dl}}''\left(R_{po} + Z_w'\right)\right] \end{aligned}$$

$$\begin{aligned} M_C'' = {} & R_t\left(Y_{Q_{dl}}'' + Y_{Q_c}''\right) \\ & + Y_{Q_c}'\left[R_t Y_{Q_{dl}}''\left(R_{po} + Z_w'\right) - Z_w''\left(1 + R_t Y_{Q_{dl}}'\right)\right] \\ & + Y_{Q_c}''\left[\left(R_t Y_{Q_{dl}}' + 1\right)\left(R_{po} + Z_w'\right) + R_t Y_{Q_{dl}}'' Z_w''\right] \end{aligned}$$

$$N_C' = R_t + \left(R_t Y_{Q_{dl}}' + 1\right)\left(R_{po} + Z_w'\right) + R_t Y_{Q_{dl}}'' Z_w''$$

$$N_C'' = R_t Y_{Q_{dl}}''\left(R_{po} + Z_w'\right) - Z_w''\left(1 + R_t Y_{Q_{dl}}'\right).$$

Warburg diffusion control

After a longer period of immersion, the impedance spectra of the coating/metal system underwent further changes due to the accumulation of metal corrosion reaction products on the metal substrate surface. Figure 9 shows the impedance spectrum of the system after immersing for 14–35 days. As can be seen, the capacitive arc no longer reduced after a prolonged immersion time, which increased instead. Magnifying observation found gradual appearance of second capacitive arc in the high-frequency region of Nyquist plot. In the Bode diagram of phase angle, the peak at the mid-low frequency region had already moved to the mid-high frequency region, which became increasingly prominent as well. This indicated the continuous expansion of corrosion reaction area at the coating/
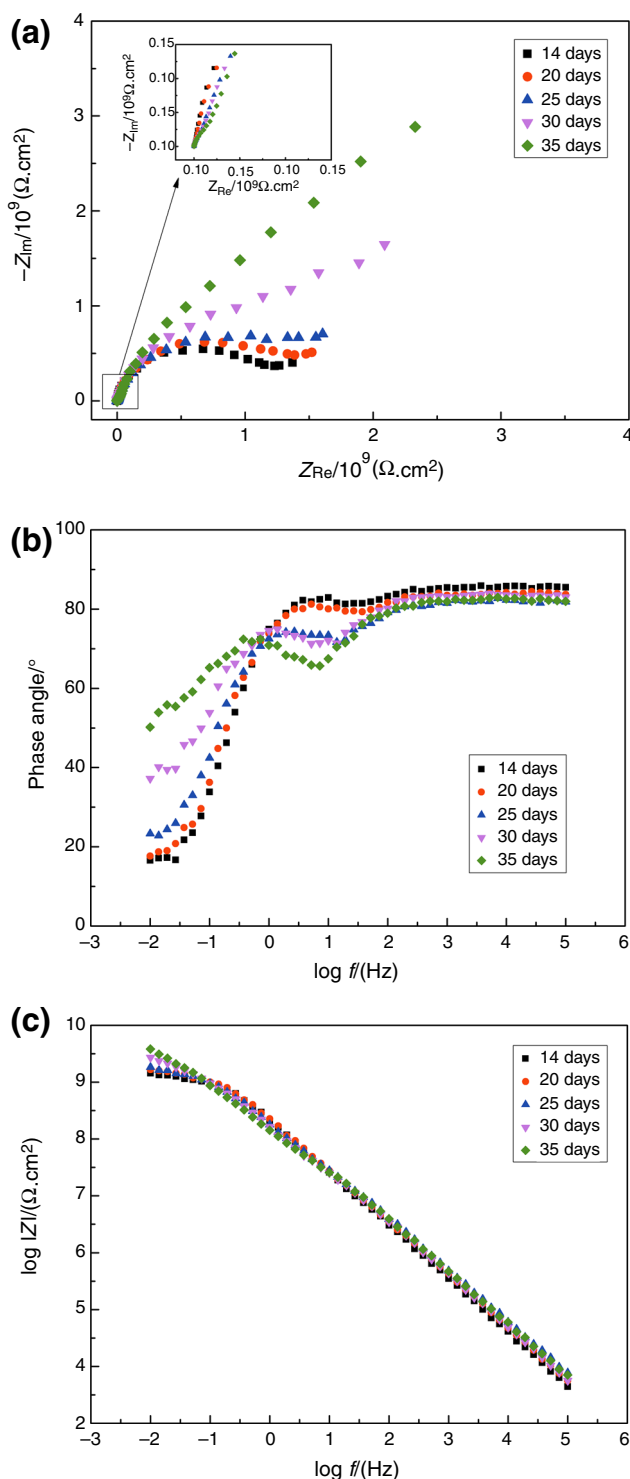

Fig. 9: Impedance spectra of coating/metal system after 14–35 days of immersion. (a) Nyquist. (b) Bode-θ. (c) Bode-$|Z|$

metal interface. An obvious diffusion process characteristic was present in the impedance spectra, i.e., straight line with a slope of about 45° in the low-frequency region (Fig. 10).
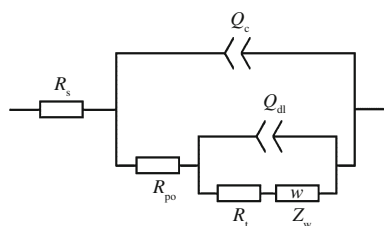
Fig. 10: Equivalent circuit model D

With the deterioration of the coating, the concentration gradient originally present within the organic coating disappeared. Meanwhile, diffusion of corrosion products was hindered due to the barrier effect of the coating. With the continuation of the corrosion reaction, corrosion products accumulated on the metal surface, thereby hindering the inward mass transfer process of corrosive particles. So, at this stage, diffusion layer was no longer located inside the coating. Instead, a new diffusion layer was formed in the reaction zone of coating/metal interface. Due to the accumulation and hindrance of corrosion products, system impedance increased with prolonged immersion time. Based on the above speculation, an equivalent circuit model D was established. The mathematical expression of impedance of equivalent circuit model D has been described in previous work.[12]

Figure 11 shows the fitting results by equivalent circuit model D with 14 days post-immersion impedance spectra of the system as an example, which were in good agreement with the experimental data.

Finite layer diffusion control

After immersion of the coating/metal system for 40 days, impedance underwent further changes. Figure 12 shows the impedance spectra of the system after 40–70 days of immersion. As can be seen from the figure, with prolonged immersion time, the capacitive arc expanded and system impedance increased. Warburg diffusion characteristics disappeared. The presence of second capacitive arc in high-frequency region was noted in the enlarged Nyquist plot. In the Bode phase angle plot, a peak in the high-frequency region was prominent. In the Bode plot of impedance modulus, two time constant characteristics were gradually revealed, indicating gradual separation between coating impedance-related time constant and electrochemical reaction-related time constant, and gradual expansion of the corroded area at the coating/metal interface.

Since the Warburg diffusion characteristics disappeared in the Nyquist plot, fitting was attempted using equivalent circuit model B, which deviated greatly

Fig. 11: Impedance spectra and fitting results of coating/ metal system after 14 days of immersion. (a) Nyquist. (b) Bode-θ

from the experimental data, as shown in Fig. 13. Taking into account that the impedance at that stage was developed from equivalent circuit model D and that Warburg impedance represented semi-infinite diffusion, the disappearance of Warburg impedance characteristics may not be due to the absence of diffusion impedance, but the result of change in diffusion type from semi-infinite diffusion into other types. Accordingly, an equivalent circuit model E was established, where O was the finite layer diffusion impedance element. Impedance of equivalent circuit model E was

$$Z_E = R_s + \cfrac{1}{Y_{Q_c} + \cfrac{1}{R_{po} + \cfrac{1}{Y_{Q_{dl}} + \cfrac{1}{R_t + Z_O}}}},$$

where

(a)

(b)

(c)

Fig. 12: Impedance spectra of coating/metal system after 40–70 days of immersion. (a) Nyquist. (b) Bode-θ. (c) Bode-|Z|
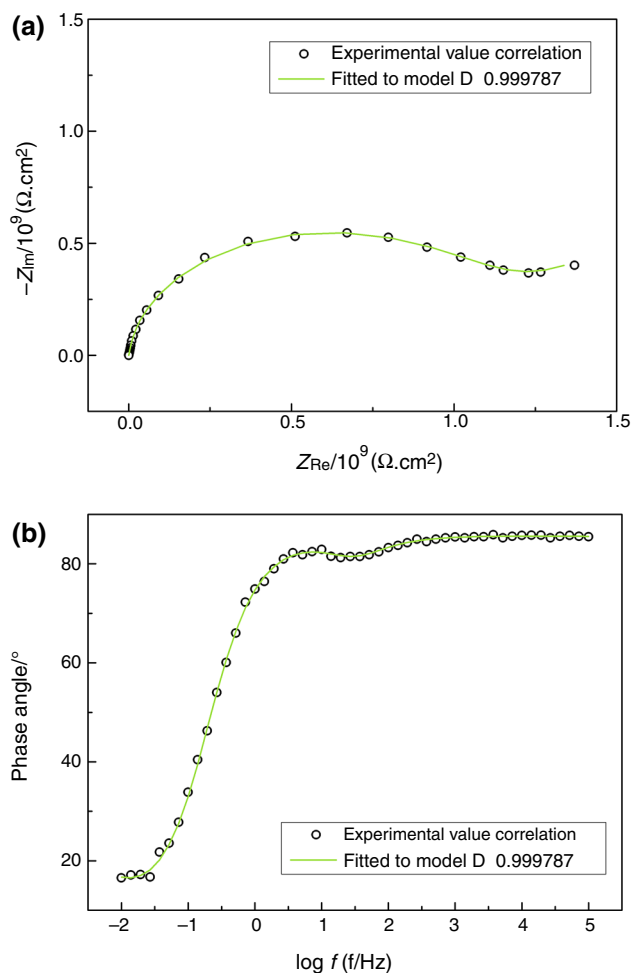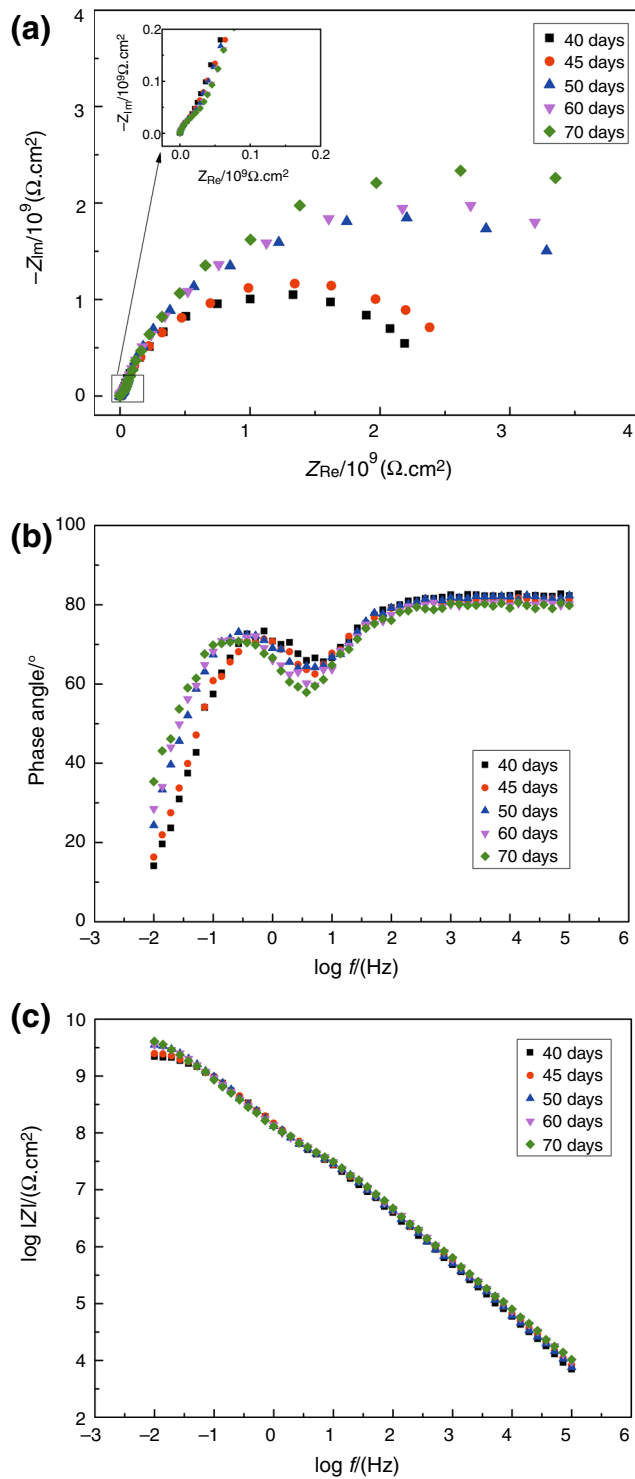

(a)

(b)

Fig. 13: Impedance spectra and fitting results of coating/metal system after 40 days of immersion. (a) Nyquist. (b) Bode-θ

$$
\begin{aligned}
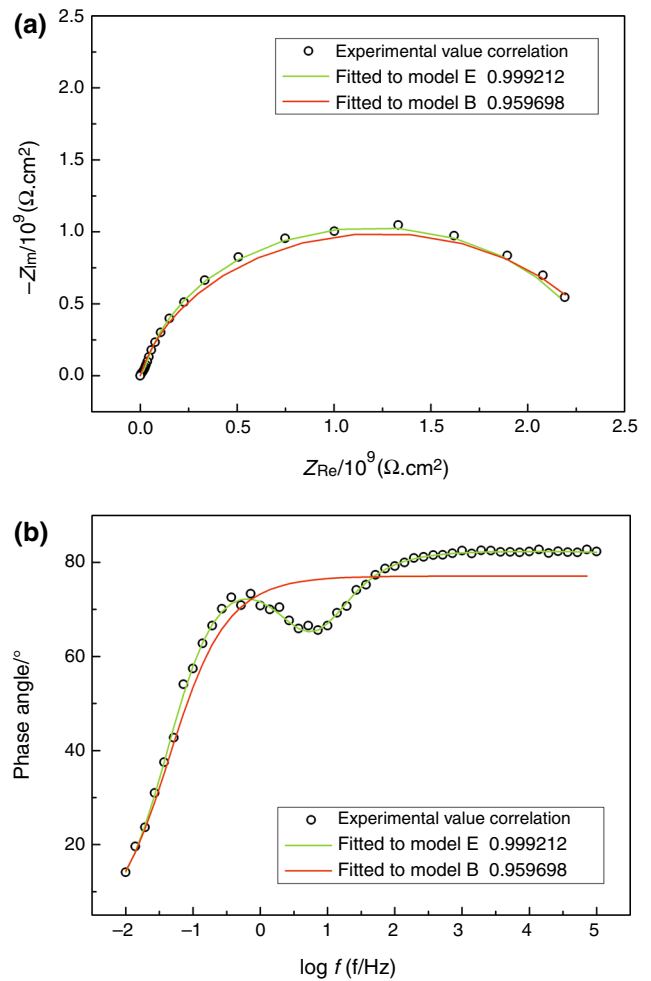Z_{\mathrm{O}} = {} & \frac{\sqrt{2}}{2}\frac{\omega^{-0.5}}{Y_{0,\mathrm{O}}}\frac{\sinh\left(\sqrt{\frac{2\omega}{D}}l\right) + \sin\left(\sqrt{\frac{2\omega}{D}}l\right)}{\cosh\left(\sqrt{\frac{2\omega}{D}}l\right) + \cos\left(\sqrt{\frac{2\omega}{D}}l\right)} \\
& - j\frac{\sqrt{2}}{2}\frac{\omega^{-0.5}}{Y_{0,\mathrm{O}}}\frac{\sinh\left(\sqrt{\frac{2\omega}{D}}l\right) - \sin\left(\sqrt{\frac{2\omega}{D}}l\right)}{\cosh\left(\sqrt{\frac{2\omega}{D}}l\right) + \cos\left(\sqrt{\frac{2\omega}{D}}l\right)} \\
= {} & Z'_{\mathrm{O}} - jZ''_{\mathrm{O}},
\end{aligned}
$$

where l was the thickness of the finite diffusion layer and D was the diffusion coefficient. By separating real part and imaginary parts, impedance Z_{E} could be
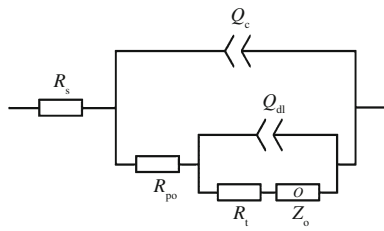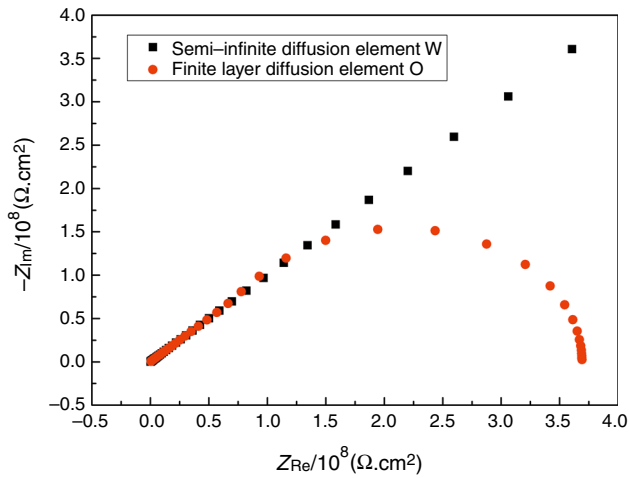
Fig. 14: Equivalent circuit model E

Fig. 15: Warburg impedance and finite layer diffusion impedance

$$Z_{\mathrm{E}} = R_{\mathrm{s}} + \frac{M'_{\mathrm{E}} N'_{\mathrm{E}} + M''_{\mathrm{E}} N''_{\mathrm{E}}}{M'^2_{\mathrm{E}} + M''^2_{\mathrm{E}}} - j \frac{N'_{\mathrm{E}} M''_{\mathrm{E}} - N''_{\mathrm{E}} M'_{\mathrm{E}}}{M'^2_{\mathrm{E}} + M''^2_{\mathrm{E}}},$$

where

$$\begin{aligned}
M'_{\mathrm{E}} &= 1 + \left(R_t + Z'_{\mathrm{O}}\right) Y'_{Q_{\mathrm{dl}}} + Z''_{\mathrm{O}} Y''_{Q_{\mathrm{dl}}} \\
&\quad - Y''_{Q_c} \left\{ R_{\mathrm{po}} \left[\left(R_t + Z'_{\mathrm{O}}\right) Y''_{Q_{\mathrm{dl}}} - Z''_{\mathrm{O}} Y'_{Q_{\mathrm{dl}}} \right] \right. \\
&\quad \left. - Z''_{\mathrm{O}} \right\} + Y'_{Q_c} \left\{ R_t + R_{\mathrm{po}} + Z'_{\mathrm{O}} + R_{\mathrm{po}} \left[\left(R_t + Z'_{\mathrm{O}}\right) Y'_{Q_{\mathrm{dl}}} \right. \right. \\
&\quad \left. \left. + Z''_{\mathrm{O}} Y''_{Q_{\mathrm{dl}}} \right] \right\}
\end{aligned}$$

$$\begin{aligned}
M''_{\mathrm{E}} &= \left(R_t + Z'_{\mathrm{O}}\right) Y''_{Q_{\mathrm{dl}}} - Z''_{\mathrm{O}} Y'_{Q_{\mathrm{dl}}} \\
&\quad + Y'_{Q_c} \left\{ R_{\mathrm{po}} \left[\left(R_t + Z'_{\mathrm{O}}\right) Y''_{Q_{\mathrm{dl}}} - Z''_{\mathrm{O}} Y'_{Q_{\mathrm{dl}}} \right] \right. \\
&\quad \left. - Z''_{\mathrm{O}} \right\} + Y''_{Q_c} \left\{ R_t + R_{\mathrm{po}} + Z'_{\mathrm{O}} + R_{\mathrm{po}} \left[\left(R_t + Z'_{\mathrm{O}}\right) Y'_{Q_{\mathrm{dl}}} \right. \right. \\
&\quad \left. \left. + Z''_{\mathrm{O}} Y''_{Q_{\mathrm{dl}}} \right] \right\}
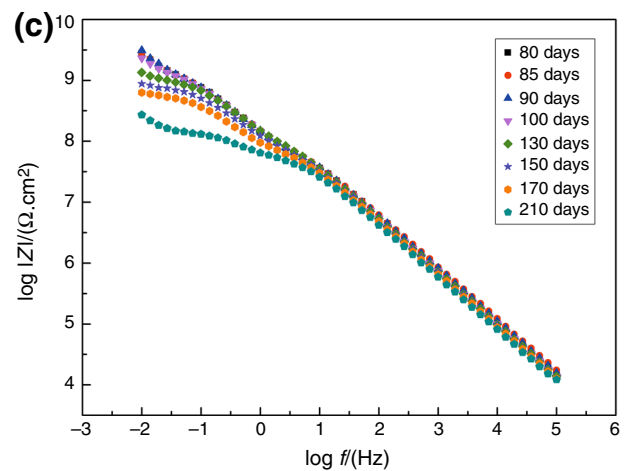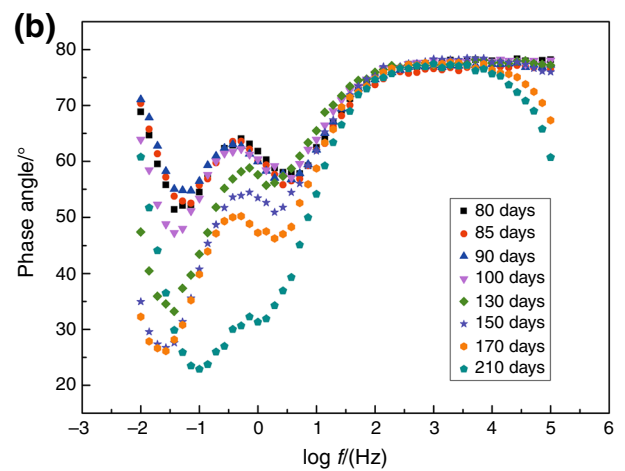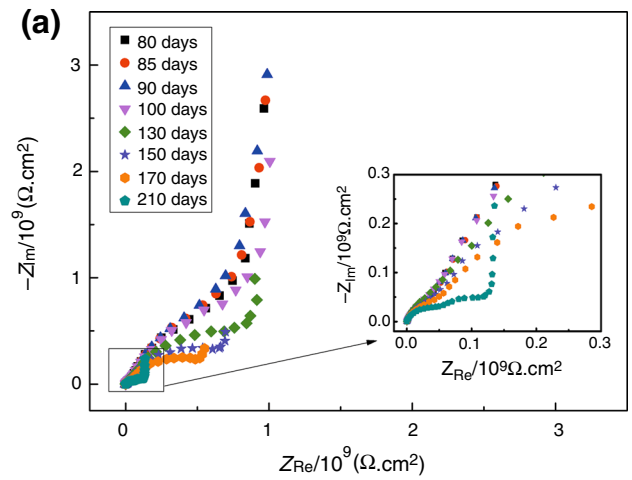\end{aligned}$$

Fig. 16: Impedance spectra of coating/metal system after 80–210 days of immersion. (a) Nyquist. (b) Bode-θ. (c) Bode-|Z|

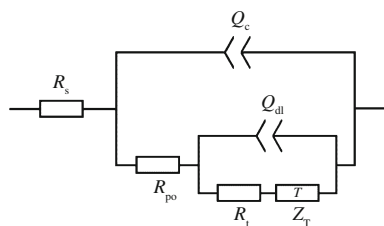**Fig. 17: Equivalent circuit model F**

$$N_{\mathrm{E}}' = R_t + R_{\mathrm{po}} + Z_{\mathrm{O}}' + R_{\mathrm{po}}\left[\left(R_t + Z_{\mathrm{O}}'\right)Y_{Q_{\mathrm{dl}}}' + Z_{\mathrm{O}}''Y_{Q_{\mathrm{dl}}}''\right]$$

$$N_{\mathrm{E}}'' = R_{\mathrm{po}}\left[\left(R_t + Z_{\mathrm{O}}'\right)Y_{Q_{\mathrm{dl}}}'' - Z_{\mathrm{O}}''Y_{Q_{\mathrm{dl}}}'\right] - Z_{\mathrm{O}}''.$$

Fitting results using equivalent circuit model E agreed well with the experimental data, as shown in Fig. 13. Theoretical topologies of Warburg impedance and finite layer diffusion impedance are shown in Fig. 15. Finite layer diffusion impedance changed from a straight line into a limited sized arc in the low-frequency end. Thus, in Fig. 14a, the 45° straight line representing Warburg impedance disappeared in the low-frequency end, which was an arc visually. The appearance of finite layer diffusion impedance element O was the result of difficulties in outward diffusion of corrosion products and inward diffusion of corrosive particles caused by clogging of micropores or defects within the coating by corrosion products. This also explains why impedance at this stage gradually increased with prolonged immersion time.

Barrier layer diffusion control

Figure 16 shows the impedance of coating after 80–210 days of immersion. As can be seen, impedance first increased and then decreased with prolonged immersion time, indicating that the impedance increasing effect caused by accumulation and hindrance of corrosion products had reached an extreme. System impedance began to decrease gradually with the further permeation of corrosive media and progression of corrosion reaction (Fig. 17). Even so, the impedance modulus remained over 10^8 orders of magnitude in the low-frequency region, with good protection property. In addition, Nyquist plot exhibited marked barrier layer diffusion characteristics, that is, a straight line nearly perpendicular to the real axis appeared in the low-frequency end. This was due to the micropores and defects in the coating basically being blocked by the corrosion products. An equivalent circuit model F was established, where T was the impedance layer diffusion element. Impedance of equivalent circuit model F was

$$Z_{\mathrm{F}} = R_{\mathrm{s}} + \cfrac{1}{Y_{Q_{\mathrm{c}}} + \cfrac{1}{R_{\mathrm{po}} + \cfrac{1}{Y_{Q_{\mathrm{dl}}} + \frac{1}{R_t + Z_{\mathrm{T}}}}}},$$

where

$$\begin{aligned} Z_{\mathrm{T}} &= \frac{\sqrt{2}}{2}\frac{\omega^{-0.5}}{Y_{0,\mathrm{T}}}\frac{\sinh\left(\sqrt{\frac{2\omega}{D}}l\right) - \sin\left(\sqrt{\frac{2\omega}{D}}l\right)}{\cosh\left(\sqrt{\frac{2\omega}{D}}l\right) - \cos\left(\sqrt{\frac{2\omega}{D}}l\right)} \\ &\quad - j\frac{\sqrt{2}}{2}\frac{\omega^{-0.5}}{Y_{0,\mathrm{T}}}\frac{\sinh\left(\sqrt{\frac{2\omega}{D}}l\right) + \sin\left(\sqrt{\frac{2\omega}{D}}l\right)}{\cosh\left(\sqrt{\frac{2\omega}{D}}l\right) - \cos\left(\sqrt{\frac{2\omega}{D}}l\right)} \\ &= Z_{\mathrm{T}}' - jZ_{\mathrm{T}}'' \end{aligned}$$

where l was the thickness of the finite diffusion layer and D was the diffusion coefficient. By separating the real part and imaginary parts, impedance Z_{F} could be

$$Z_{\mathrm{F}} = R_{\mathrm{s}} + \frac{M_{\mathrm{F}}'N_{\mathrm{F}}' + M_{\mathrm{F}}''N_{\mathrm{F}}''}{M_{\mathrm{F}}'^2 + M_{\mathrm{F}}''^2} - j\frac{N_{\mathrm{F}}'M_{\mathrm{F}}'' - N_{\mathrm{F}}''M_{\mathrm{F}}'}{M_{\mathrm{F}}'^2 + M_{\mathrm{F}}''^2},$$

where

$$\begin{aligned} M_{\mathrm{F}}' &= 1 + \left(R_t + Z_{\mathrm{T}}'\right)Y_{Q_{\mathrm{dl}}}' + Z_{\mathrm{T}}''Y_{Q_{\mathrm{dl}}}'' \\ &\quad - Y_{Q_{\mathrm{c}}}''\left\{R_{\mathrm{po}}\left[\left(R_t + Z_{\mathrm{T}}'\right)Y_{Q_{\mathrm{dl}}}'' - Z_{\mathrm{T}}''Y_{Q_{\mathrm{dl}}}'\right]\right. \\ &\quad \left. - Z_{\mathrm{T}}''\right\} + Y_{Q_{\mathrm{c}}}'\left\{R_t + R_{\mathrm{po}} + Z_{\mathrm{T}}'\right. \\ &\quad \left. + R_{\mathrm{po}}\left[\left(R_t + Z_{\mathrm{T}}'\right)Y_{Q_{\mathrm{dl}}}' + Z_{\mathrm{T}}''Y_{Q_{\mathrm{dl}}}''\right]\right\} \end{aligned}$$

$$\begin{aligned} M_{\mathrm{F}}'' &= \left(R_t + Z_{\mathrm{T}}'\right)Y_{Q_{\mathrm{dl}}}'' - Z_{\mathrm{T}}''Y_{Q_{\mathrm{dl}}}' \\ &\quad + Y_{Q_{\mathrm{c}}}'\left\{R_{\mathrm{po}}\left[\left(R_t + Z_{\mathrm{T}}'\right)Y_{Q_{\mathrm{dl}}}'' - Z_{\mathrm{T}}''Y_{Q_{\mathrm{dl}}}'\right]\right. \\ &\quad \left. - Z_{\mathrm{T}}''\right\} + Y_{Q_{\mathrm{c}}}''\left\{R_t + R_{\mathrm{po}} + Z_{\mathrm{T}}' + R_{\mathrm{po}}\left[\left(R_t + Z_{\mathrm{T}}'\right)Y_{Q_{\mathrm{dl}}}'\right.\right. \\ &\quad \left.\left. + Z_{\mathrm{T}}''Y_{Q_{\mathrm{dl}}}''\right]\right\} \end{aligned}$$

$$N_{\mathrm{F}}' = R_t + R_{\mathrm{po}} + Z_{\mathrm{T}}' + R_{\mathrm{po}}\left[\left(R_t + Z_{\mathrm{T}}'\right)Y_{Q_{\mathrm{dl}}}' + Z_{\mathrm{T}}''Y_{Q_{\mathrm{dl}}}''\right]$$

$$N_{\mathrm{F}}'' = R_{\mathrm{po}}\left[\left(R_t + Z_{\mathrm{T}}'\right)Y_{Q_{\mathrm{dl}}}'' - Z_{\mathrm{T}}''Y_{Q_{\mathrm{dl}}}'\right] - Z_{\mathrm{T}}''$$

Fitting of impedance data using the equivalent circuit model F can yield good results, as shown in Fig. 18.
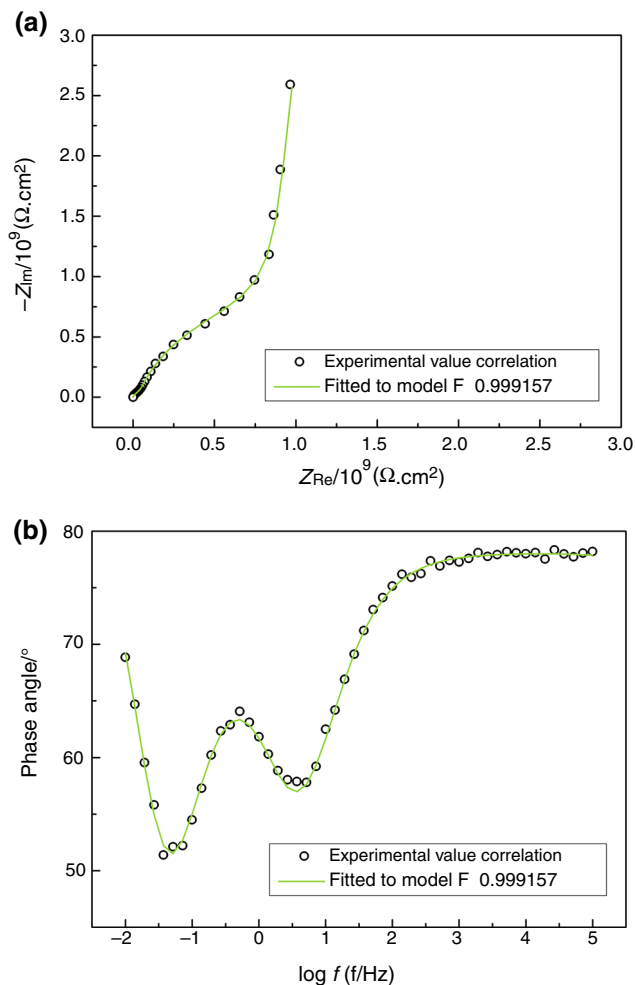
Results of Chi-squared test are displayed in Table 2 which contained results of all the impedance spectroscopies fitted by each equivalent circuit. Equivalent

circuits which had minimum Chi-square values were chosen to describe the corresponding impedance spectroscopy. In addition, equivalent circuit B was established for comparison with equivalent circuit C and discussion of diffusion impedance in the coatings.

Water transport behavior in coating

Coating capacitance and water uptake

The protective effects of the coating included the mechanical protection of metal and the prevention of water, oxygen, and other corrosive medium entry to the coating/metal interface. Since the diffusion coefficients of other particles in organic coatings are far


Fig. 18: Impedance spectra and fitting results of coating/metal system after 80 days of immersion. (a) Nyquist. (b) Bode-θ
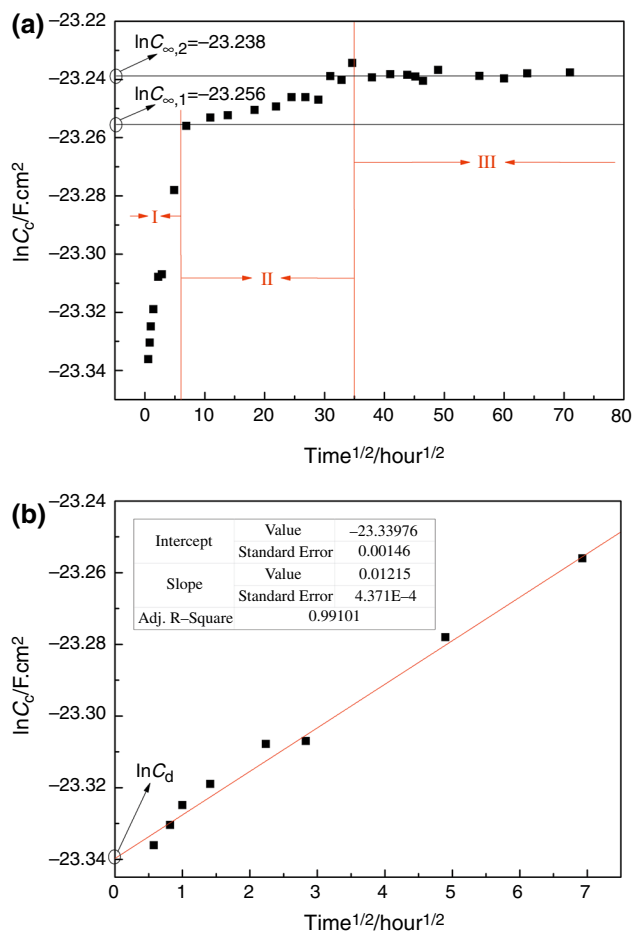
Fig. 19: Capacitance–time curve of coating/metal system. (a) Entire immersion period. (b) Linear region

Table 2: Chi-Squared Test Results of All the Impedance Spectroscopies Fitted by Each Equivalent Circuit

Impedance	Figure 4	Figure 6	Figure 11	Figure 13	Figure 18
Equivalent circuit					
A	2.03E−13	1.56E−04	4.65E−03	2.49E−02	7.48E−02
B	6.77E−13	4.84E−05	4.99E−03	2.67E−02	6.31E−03
C	2.54E−13	3.03E−10	9.65E−04	1.72E−06	7.69E−03
D	2.43E−13	1.68E−04	9.61E−04	1.70E−06	9.29E−03
E	2.67E−13	1.04E−01	9.85E−04	1.65E−06	5.55E−03
F	4.89E−13	1.04E−01	9.85E−04	1.67E−06	5.40E−03
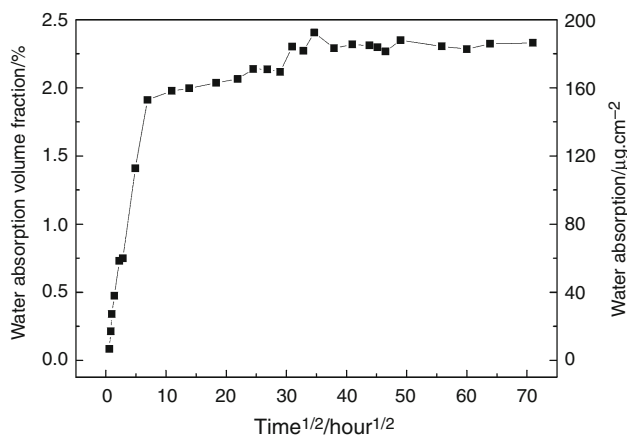
Fig. 20: Water absorption volume fraction and total water absorption amount of coating

smaller than the diffusion coefficient of water, the study of water transport in organic coatings is of practical significance.[14] A relatively fast and reliable method for studying water transport in organic coatings is the capacitance method.[15] As the coating capacitance had a functional relationship with the water permeation into the coating, the water absorption characteristics of water immersed coating could be studied based on the changes in coating capacitance.[16]

By fitting impedance data, capacitance of coating C_c at different immersion stages could be obtained, and the capacitance-time curve ($\ln C_c \sim t^{1/2}$) could be plotted using natural logarithm of capacitance $\ln C_c$ and square root of immersion time $t^{1/2}$, as shown in Fig. 19. In Fig. 19a, coating capacitance presented two-stage absorption characteristics with prolonged immersion time. A period of fast absorption was followed by a period of slow absorption until ultimately reaching saturation. During the early stage of immersion (0–40 h), coating capacitance increased rapidly in a linear fashion over time, as shown in Fig. 19b, and the slope was approximately 0.012. This suggested that the water in the corrosive medium permeated inside the organic coating through micropores in the coating. Due to the water permeation, coating capacitance increased rapidly. The natural logarithm of coating capacitance exhibited a linear variation with the square root of immersion time, indicating that the water permeated into the coating in a uniform manner, and that the water transport behavior obeyed Fick's law. By fitting the linear zone data, the intercept of straight line at $t = 0$ could be obtained as -23.34 which was the dry coating capacitance C_d. After immersion for about 40 h, growth of coating capacitance slowed down. This stage was a non-Fickian diffusion stage, which lasted about 1300 h. The occurrence of non-Fickian diffusion may be due to the structural relaxation of coating polymers. Afterward, the coating capacitance maintained a relatively stable value, which was the capacitance $C_{\infty,2}$ of coating at water saturation. Coating

capacitance at the turning point between Fickian diffusion and non-Fickian diffusion was denoted by $C_{\infty,1}$, which was the maximum increase in coating capacitance caused by the Fickian diffusion way of water absorption.

Relative permittivity of dry coating ε_d and water diffusion coefficient in coating D could be calculated based on the linear region slope $\frac{d\ln C_c}{d\sqrt{t}}$, dry coating capacitance C_d, and capacitance at water saturation C_∞. ε_d value was 6.601, which was within the relative permittivity range of dry coating 3–8 reported in the literature.[17–19] D value was 2.95×10^{-10} cm^2/s, which was consistent with the water diffusion coefficient range of coatings with good protective properties 10^{-8}–10^{-12} cm^2/s reported in the literature, while confirming the validity of impedance data.[20–23]

Fickian diffusion duration t_s can be calculated by the following formula.[24,25] $t_s \approx 34$ h obtained by the formula with the water diffusion coefficient in coating was basically consistent with the time of turning point between Fickian diffusion and non-Fickian diffusion as shown in Fig. 19. This indicated from another aspect that the water diffusion behavior in the coating during the early immersion stage obeyed Fick's law.

$$t_s = \frac{L^2}{D}$$

Figure 20 shows the water absorption volume fraction υ, and total water absorption amount M of coating, υ calculated by $\upsilon = \ln(C_c/C_d)/\ln\varepsilon_w$, and M is calculated by $M(t) = SL\rho_w \ln(C_c/C_d)/\ln\varepsilon_w$. When the coating was saturated with water, the water absorption volume fraction was 2.3%, and the total water absorption amount was around 185 μg/cm^2, which was lower than the range of water absorption volume fraction of epoxy-based coatings 2.0–15.98% reported in the literature,[26–29] indicating good water resistance and protective properties of the coating.

Absorbing kinetic equation

In previous work, we calculated the kinetic equation which was applicable only before water permeation into the coating/metal interface:[12]

$$\varphi(z,t) = \frac{2}{\sqrt{\pi}} \int_{\frac{z}{2\sqrt{Dt}}}^{+\infty} e^{-\eta^2} d\eta = erfc\left(\frac{z}{2\sqrt{Dt}}\right)$$

After water permeated into the coating/metal interface, the equation was no longer applicable. This study will continue to calculate the kinetic equation which can reflect the whole Fick diffusion process of water.

In the Fickian diffusion stage, water absorbing process of coating can be described by Fick's laws.[30] It was assumed that φ is the ratio of water volume fraction υ to its saturated value υ_∞, $\varphi = \upsilon/\upsilon_\infty$ and

$0 \leq \varphi \leq 1$. In Fick's law, t was time; z was the distance to coating/substrate interface; $z = 0$ at the coating/substrate interface, and $z = L$ at the coating surface which was different from the calculation process of above kinetic equation in our previous works in order to facilitate the calculation.[12] φ was a function $\varphi = \varphi(z, t)$ of t and z. J was the diffusion flux.

$$J = -D\frac{d\varphi}{dz} \tag{1}$$

$$\frac{\partial \varphi}{\partial t} = D\frac{\partial^2 \varphi}{\partial z^2} \tag{2}$$

The above formula satisfied the following boundary conditions. When $t = 0$, volume fraction of water within all parts of coating was 0. At $z = L$ on the coating surface, volume fraction of water was always saturated. At $z = 0$, rate of change in volume fraction of water with z was 0.

Boundary conditions I $\quad \varphi(z, 0) = 0 \tag{3}$

Boundary conditions II $\quad \varphi(L, t) = 1 \tag{4}$

Boundary conditions III $\quad \dfrac{\partial}{\partial z}\varphi(0, t) = 0 \tag{5}$

Function $\varphi(z, t)$ was Laplace transformed to obtain the image function $\tilde{\varphi}(z, s)$, where s was the parametric variable.[31]

$$\tilde{\varphi}(z, s) = \mathcal{L}[\varphi(z, t)] = \int_0^{+\infty} \varphi(z, t)e^{-st}dt \tag{6}$$

According to the boundary conditions II and III, the following could be obtained:

Boundary conditions IV $\quad \tilde{\varphi}(L, s) = \dfrac{1}{s} \tag{7}$

Boundary conditions V $\quad \dfrac{\partial}{\partial z}\tilde{\varphi}(0, s)$
$$= \frac{\partial}{\partial z}\int_0^{+\infty} \varphi(0, t)e^{-st}dt = 0 \tag{8}$$

Derivative of $\varphi(z, t)$ was Laplace transformed to obtain the following combined with the boundary conditions I:

$$\mathcal{L}\left[\frac{\partial}{\partial t}\varphi(z, t)\right] = s\tilde{\varphi} - s\varphi_{(t=0)} = s\tilde{\varphi} \tag{9}$$

Thus, Fick's second law, i.e., Laplace transform of equation (2) was

$$\frac{d^2\tilde{\varphi}}{dz^2} - \frac{s}{D}\tilde{\varphi} = 0 \tag{10}$$

This was a typical second-order linear homogeneous equation with constant coefficients in the form of $\frac{d^2y}{dx^2} + p\frac{dy}{dx} + qy = 0$.

Let

$$\tilde{\varphi} = e^{rz} \tag{11}$$

Its second derivative was

$$\frac{d^2\tilde{\varphi}}{dz^2} = r^2 e^{rz} \tag{12}$$

Thus, equation (10) can be written as follows:

$$r^2 e^{rz} - \frac{s}{D}e^{rz} = 0 \tag{13}$$

By solving (13), we obtain

$$r = \pm\sqrt{\frac{s}{D}}. \tag{14}$$

Therefore, solution of equation (10) was the following formula, where k_1 and k_2 were the coefficients.

$$\tilde{\varphi} = k_1 e^{\sqrt{\frac{s}{D}}z} + k_2 e^{-\sqrt{\frac{s}{D}}z} \tag{15}$$

Partial derivative of $\tilde{\varphi}$ was

$$\frac{\partial\tilde{\varphi}}{\partial z} = k_1\sqrt{\frac{s}{D}}e^{\sqrt{\frac{s}{D}}z} - k_2\sqrt{\frac{s}{D}}e^{-\sqrt{\frac{s}{D}}z} \tag{16}$$

$k_1 = k_2$ can be obtained from the boundary conditions V; hence (15) can be written as follows:

$$\tilde{\varphi} = k_1\left(e^{\sqrt{\frac{s}{D}}z} + e^{-\sqrt{\frac{s}{D}}z}\right) = 2k_1\cosh\left(\sqrt{\frac{s}{D}}z\right) \tag{17}$$

The following could be obtained based on boundary conditions IV:

$$\tilde{\varphi}(L, s) = 2k_1\cosh\left(\sqrt{\frac{s}{D}}L\right) = \frac{1}{s} \tag{18}$$

$$k_1 = \frac{1}{2s}\frac{1}{\cosh\left(\frac{L}{\sqrt{D}}\sqrt{s}\right)} \tag{19}$$

By introducing (19) into (17), we obtain

$$\tilde{\varphi} = \frac{1}{s}\frac{\cosh\left(\frac{z}{\sqrt{D}}\sqrt{s}\right)}{\cosh\left(\frac{L}{\sqrt{D}}\sqrt{s}\right)} \tag{20}$$

Apparently, $s = s_0 = 0$ was the first-order pole of $\tilde{\varphi}$; hence, we could let

$$\tilde{\varphi}(z,s) = \frac{1}{s - s_0} f(z,s) \tag{21}$$

Taylor series expansion of $f(z, s)$ at s_0 was equation (22); moreover, $\alpha_0 = f(z, s_0) \neq 0$.

$$f(z,s) = \sum_{n=0}^{+\infty} \alpha_n (s - s_0)^n \tag{22}$$

where

$$\alpha_n = \frac{f^{(n)}(z, s_0)}{n!} \quad (n = 0, 1, 2, \ldots) \tag{23}$$

Laurent series expansion of $\tilde{\varphi}(z,s)$ at s_0 was

$$\tilde{\varphi}(z,s) = \sum_{n=-\infty}^{+\infty} c_n (s - s_0)^n, \tag{24}$$

where

$$c_n = \frac{1}{2\pi i} \oint_C \frac{\tilde{\varphi}(z, \mu)}{(\mu - s_0)^{n+1}} d\mu \quad (n = 0, \pm 1, \pm 2, \ldots) \tag{25}$$

Obviously, in the Laurent series of $\tilde{\varphi}(z,s)$, the coefficient of $1/(s - s_0)$ equaled $f(z, s_0)$. Thus, residue of $\tilde{\varphi}(z,s)$ at s_0 was

$$\mathrm{Res}[\tilde{\varphi}(z,s), s_0] = \lim_{s \to s_0} (s - s_0)\tilde{\varphi}(z,s) = \lim_{s \to 0} s\tilde{\varphi}(z,s) \tag{26}$$

Hence,

$$\mathrm{Res}[e^{st}\tilde{\varphi}(z,s), s_0] = \lim_{s \to 0} se^{st}\tilde{\varphi}(z,s) \tag{27}$$

When $\cosh\left(\frac{L}{\sqrt{D}}\sqrt{s}\right) = 0$, $e^{\frac{L}{\sqrt{D}}\sqrt{s}} = -e^{-\frac{L}{\sqrt{D}}\sqrt{s}}$, so $e^{2\frac{L}{\sqrt{D}}\sqrt{s}} = -1$. Obviously, $2\frac{L}{\sqrt{D}}\sqrt{s}$ should be a plural. Let

$$2\frac{L}{\sqrt{D}}\sqrt{s} = p + qi \tag{28}$$

Then

$$e^{p+qi} = e^p(\cos q + i\sin q) = -1 \tag{29}$$

From the above equation, we could obtain

$$p = 0, \quad q = (2n - 1)\pi \tag{30}$$

Therefore,

$$2\frac{L}{\sqrt{D}}\sqrt{s} = (2n - 1)\pi \tag{31}$$

From the above equation, we could obtain

$$\sqrt{s} = \sqrt{s_n} = \frac{\sqrt{D}}{L}\left(n - \frac{1}{2}\right)\pi i (n = 1, 2, \ldots) \tag{32}$$

$$s = s_n = -\frac{D}{L^2}\left(n - \frac{1}{2}\right)^2 \pi^2 (n = 1, 2, \ldots) \tag{33}$$

Therefore, $s = s_n$ was the first-order pole of $\tilde{\varphi}$. Residue

$$\begin{aligned}
\mathrm{Res}[e^{st}\tilde{\varphi}(z,s), s_n] &= \lim_{s \to s_n} (s - s_n)e^{st}\tilde{\varphi}(z,s) \\
&= e^{s_n t} \frac{\cosh\left(\frac{z}{\sqrt{D}}\sqrt{s_n}\right)}{s_n} \lim_{s \to s_n} \frac{s - s_n}{\cosh\left(\frac{L}{\sqrt{D}}\sqrt{s}\right)}
\end{aligned} \tag{34}$$

According to L'Hospital's rule,

$$\begin{aligned}
\lim_{s \to s_n} \frac{s - s_n}{\cosh\left(\frac{L}{\sqrt{D}}\sqrt{s}\right)} &= \lim_{s \to s_n} \frac{(s - s_n)'}{\left[\cosh\left(\frac{L}{\sqrt{D}}\sqrt{s}\right)\right]'} \\
&= \lim_{s \to s_n} \frac{2\sqrt{s}}{\frac{L}{\sqrt{D}}\sinh\left(\frac{L}{\sqrt{D}}\sqrt{s}\right)} = \frac{2\sqrt{s_n}}{\frac{L}{\sqrt{D}}\sinh\left(\frac{L}{\sqrt{D}}\sqrt{s_n}\right)}
\end{aligned} \tag{35}$$

By (29) and (32), we could obtain

$$\begin{aligned}
\sinh\left(\frac{L}{\sqrt{D}}\sqrt{s_n}\right) &= \sinh\left[\left(n - \frac{1}{2}\right)\pi i\right] \\
&= \frac{1}{2}\left[e^{\left(n-\frac{1}{2}\right)\pi i} - e^{-\left(n-\frac{1}{2}\right)\pi i}\right] = \frac{1}{2}\left\{\cos\left[\left(n - \frac{1}{2}\right)\pi\right]\right. \\
&+ i\sin\left[\left(n - \frac{1}{2}\right)\pi\right] - \cos\left[-\left(n - \frac{1}{2}\right)\pi\right] \\
&\left. - i\sin\left[-\left(n - \frac{1}{2}\right)\pi\right]\right\} = (-1)^{n+1} i
\end{aligned} \tag{36}$$

$$\begin{aligned}
\cosh\left(\frac{z}{\sqrt{D}}\sqrt{s_n}\right) &= \frac{1}{2}\left[e^{\frac{z}{L}\left(n-\frac{1}{2}\right)\pi i} + e^{-\frac{z}{L}\left(n-\frac{1}{2}\right)\pi i}\right] \\
&= \frac{1}{2}\left\{\cos\left[\frac{z}{L}\left(n - \frac{1}{2}\right)\pi\right] + i\sin\left[\frac{z}{L}\left(n - \frac{1}{2}\right)\pi\right]\right. \\
&\left. + \cos\left[-\frac{z}{L}\left(n - \frac{1}{2}\right)\pi\right] + i\sin\left[-\frac{z}{L}\left(n - \frac{1}{2}\right)\pi\right]\right\} \\
&= \cos\left[\frac{z}{L}\left(n - \frac{1}{2}\right)\pi\right]
\end{aligned} \tag{37}$$

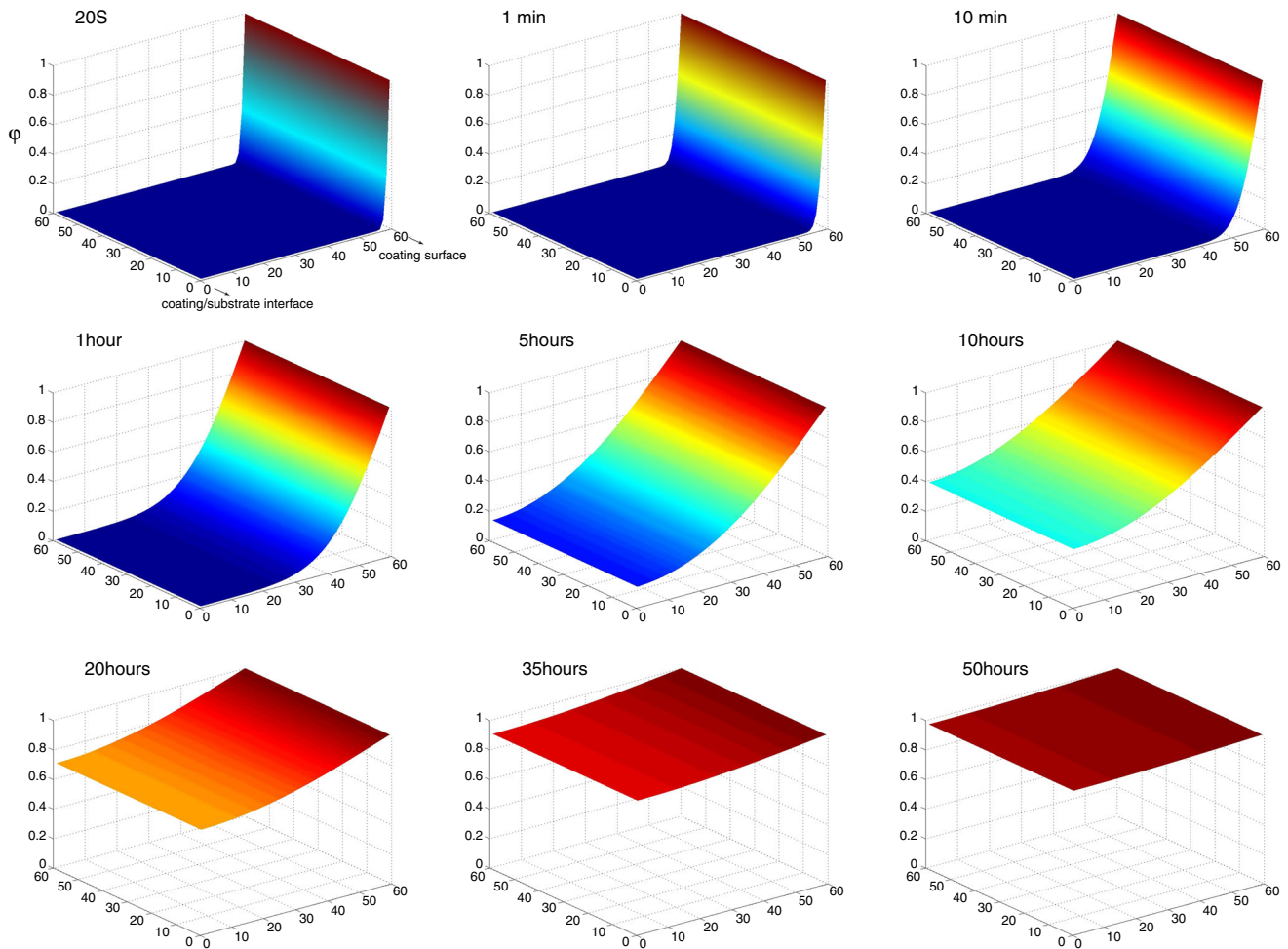By introducing (32) and (36) into (35), we could obtain

Fig. 21: Three-dimensional images of water distribution in the first 50 h

$$\lim_{s \to s_n} \frac{s - s_n}{\cosh\left(\frac{L}{\sqrt{D}}\sqrt{s}\right)} = (-1)^{n+1}\frac{D}{L^2}(2n-1)\pi$$
$$(n = 1, 2, \ldots)$$
(38)

By introducing (33), (37), and (38) into (34), we could obtain

$$\text{Res}[e^{st}\tilde{\varphi}(z,s),s_n] = \frac{(-1)^n}{(2n-1)\pi}$$
$$\cdot 4\cos\left[\frac{z}{L}\left(n-\frac{1}{2}\right)\pi\right]e^{-\frac{Dt}{L^2}\left(n-\frac{1}{2}\right)^2\pi^2}$$
$$(n = 1, 2, \ldots)$$
(39)

According residue method, inverse Laplace transform of $\tilde{\varphi}(z,s)$ can be calculated by residues of all poles of function $e^{st}\tilde{\varphi}(z,s)$. Therefore, inverse Laplace transform of $\tilde{\varphi}(z,s)$ was

$$\varphi(z,t) = \mathcal{L}^{-1}[\tilde{\varphi}(z,s)]$$
$$= \text{Res}[e^{st}\tilde{\varphi}(z,s),s_0] + \text{Res}[e^{st}\tilde{\varphi}(z,s),s_n]$$
$$= 1 + \frac{4}{\pi}\sum_{n=1}^{+\infty}\frac{(-1)^n}{2n-1}\cos\left[\frac{z}{L}\left(n-\frac{1}{2}\right)\pi\right]e^{-\frac{Dt}{L^2}\left(n-\frac{1}{2}\right)^2\pi^2}$$
(40)

Equation (40) was precisely the kinetic equation for water absorption volume fraction of coating. The kinetic equation was shown in the form of infinite sum. When $n \geq 100,000$, φ could be accurate to six decimal places, and the error caused by n was no longer observed on the image of the equation.

Three-dimensional images of water distribution with arbitrary timings and from the coating cross-section of view were obtained via transforming the equation into programs. Superimposed were these three-dimensional images in chronological order and the dynamic change graph of water distribution was obtained. Figure 19 shows the turning points of Fick diffusion and non-Fick

diffusion that was at approximately 50 h. So, three-dimensional images of water distribution in the first 50 h are displayed in Fig. 21. Water uptake was linearly correlated to square root of time; therefore, the absorption process slowed down gradually over time, which could be obtained from Fig. 21. In addition, water absorption of the coating reached about 97% of saturation value in the first 50 h which was consistent with the ratio of $C_{\infty,1}/C_{\infty,2} = 98.2\%$ as shown in Fig. 19. Therefore, the remaining approximately 3% of water absorption was contributed by the non-Fick diffusion process.

Conclusions

The evolution of the impedance model of 60 μm modified solvent-free epoxy anti-corrosion coatings used herein on the steel surface could be divided into five stages, which were initial water absorption, occurrence of corrosion and impeded absorption, Warburg diffusion control, finite layer diffusion control, and barrier layer diffusion. In the initial water absorption stage, impedance spectroscopy showed an arc of large radius, and when the immersion time increased, coating capacitance increased, and coating resistance was reduced. When corrosion occurred, the electric double layer capacitor and charge transfer resistance emerged in the equivalent circuit. In the meantime, micaceous iron oxides contained in the coating played a barrier role in diffusion within the coating, and mass transfer process became a slow procedure. In the Warburg diffusion control stage, due to the barrier effect of coatings, electrochemical reactions at coating/metal interface were controlled by the diffusion of corrosion products. At this stage, diffusion layer was no longer located inside the coating. Instead, a new diffusion layer was formed in the reaction zone of coating/metal interface. The appearance of finite layer diffusion which replaced Warburg diffusion was the result of difficulties in outward diffusion of corrosion products and inward diffusion of corrosive particles caused by clogging of micropores or defects within the coating by corrosion products. Due to the micropores and defects in the coating basically being blocked by the corrosion products, finite layer diffusion transformed into barrier layer diffusion. Water diffusion process in the coating was divided into three stages. The first stage was Fick diffusion in which natural logarithm of coating capacitance show a linear relationship with square root of time. Then Fick diffusion transformed into non-Fick diffusion, and the water absorption process slowed down. The non-Fick diffusion was followed by water saturation status and coating capacitance was steadied at a certain value. The kinetic equation of water diffusion in the coating was shown in the form of infinite sum. By transforming the dynamic equation into programs, three-dimensional images of water distribution in the coating were obtained.

References

1. Orazem, ME, Tribollet, B, *Electrochemical Impedance Spectroscopy*, Vol. 48. Wiley, New York (2011)
2. Randviir, EP, Banks, CE, "Electrochemical impedance spectroscopy: an overview of bioanalytical applications." *Anal. Methods*, **5** (5) 1098–1115 (2013)
3. Amadi, SA, Ukpaka, CP, "Performance Evaluation of Anti-corrosion Coating in an Oil Industry." *Int. J. Nov. Res. Eng. Pharm. Sci.*, **1** (03) 41–49 (2014)
4. Liu, J, et al., "Studies of Impedance Models and Water Transport Behaviours of Epoxy Coating at Hydrostatic Pressure of Seawater." *Prog. Org. Coat.*, **76** (7) 1075–1081 (2013)
5. Zhang, JT, et al., "Studies of Impedance Models and Water Transport Behaviors of Polypropylene Coated Metals in NaCl Solution." *Prog. Org. Coat.*, **49** (4) 293–301 (2001)
6. Zhang, JQ, *Electrochemical Measurement Technology*. Chemistry & Industry Press, Peking (2010)
7. Hu, JM, et al., "Determination of Water Uptake and Diffusion of Cl⁻ Ion in Epoxy Primer on Aluminum Alloys in NaCl Solution by Electrochemical Impedance Spectroscopy." *Acta. Phys. Chim. Sin.*, **46** (4) 273–279 (2003)
8. Allahar, KN, et al., "Water Transport in Multilayer Organic Coatings." *J. Electrochem. Soc.*, **155** (8) 201–208 (2008)
9. Cao, CN, *Principles of Electrochemistry of Corrosion*. Chemistry and Industry Press, Peking (2008)
10. Liu, Y, et al., "Study of the Failure Mechanism of an Epoxy Coating System Under High Hydrostatic Pressure." *Corros. Sci.*, **74** 59–70 (2013)
11. Li, RJ, *Heavy-Duty Coatings and Technology*. Chemistry & Industry Press, Peking (2014)
12. Ding, R, Jiang, JM, Gui, TJ, "Study of Impedance Model and Water Transport Behavior of Modified Solvent-Free Epoxy Anti-corrosion Coating by EIS." *J. Coat. Technol. Res.*, **13** (3) 1–15 (2016)
13. Cao, CN, Zhang, JQ, *EIS Introduction*. China Science, Peking (2002)
14. Sørensen, PA, et al., "Anticorrosive Coatings: A Review." *J. Coat. Technol Res.*, **6** (2) 135–176 (2009)
15. Zhu, CF, et al., "Studies of the Impedance Models and Water Transport Behaviors of Cathodically Polarized Coating." *Electrochim. Acta*, **56** (16) 5828–5835 (2011)
16. HaeRi, Jeon, Park, JinHwan, Shon, MinYoung, "Corrosion Protection by Epoxy Coating Containing Multi-walled Carbon Nanotubes." *J. Indus. Eng. Chem.*, **19** (3) 849–853 (2013)
17. Moreno, C, et al., "Characterization of Water Uptake by Organic Coatings Used for the Corrosion Protection of Steel as Determined from Capacitance Measurements." *Int. J. Electrochem. Sci.*, **7** 8444–8457 (2012)
18. Liu, Y, et al., "Study of the Failure Mechanism of an Epoxy Coating System Under High Hydrostatic Pressure." *Corros. Sci.*, **74** 59–70 (2013)
19. Shreepathi, S, et al., "Water Transportation Through Organic Coatings: Correlation Between Electrochemical Impedance Measurements, Gravimetry, and Water Vapor Permeability." *J. Coat. Technol. Res.*, **9** (4) 411–422 (2012)

20. Zhai, Z, et al., "Water Absorption and Mechanical Property of an Epoxy Composite Coating Containing Unoxidized Aluminum Particles." *Prog. Org. Coat.*, **87** 106–111 (2015)

21. Hornell, J, *Water Transport*. Cambridge University Press, Cambridge (2015)

22. Yuan, X, et al., "EIS Study of Effective Capacitance and Water Uptake Behaviors of Silicone-Epoxy Hybrid Coatings on Mild Steel." *Prog. Org. Coat.*, **86** 41–48 (2015)

23. Guo, XH, et al., "Study of Barrier Property of Composite Film Coated on Mg-Gd-Y Alloy by Water Diffusion." *ECS Electrochem. Lett.*, **2** (8) C27–C30 (2013)

24. Monetta, T, et al., "Protective Properties of Epoxy-Based Organic Coatings on Mild Steel." *Prog. Org. Coat.*, **21** (4) 353–369 (1993)

25. Wind, MM, Lenderink, HJW, "A Capacitance Study of Pseudo-Fickian Diffusion in Glassy Polymer Coatings." *Prog. Org. Coat.*, **28** (4) 239–250 (1996)

26. Ramezanzadeh, B, Attar, MM, "Studying the Corrosion Resistance and Hydrolytic Degradation of an Epoxy Coating Containing ZnO Nanoparticles." *Mater. Chem. Phys.*, **130** (3) 1208–1219 (2011)

27. Skale, S, et al., "Electrochemical Impedance Studies of Corrosion Protected Surfaces Covered by Epoxy Polyamide Coating Systems." *Prog. Org. Coat.*, **62** (4) 387–392 (2008)

28. Legghe, E, et al., "Correlation Between Water Diffusion and Adhesion Loss: Study of an Epoxy Primer on Steel." *Prog. Org. Coat.*, **66** (3) 276–280 (2009)

29. Fredj, N, et al., "Evidencing Antagonist Effects of Water Uptake and Leaching Processes in Marine Organic Coatings by Gravimetry and EIS." *Prog. Org. Coat.*, **67** (3) 287–295 (2010)

30. Fu, XC, Shen, WX, et al., *Physical Chemistry*. Higher Education, Peking (2006)

31. Luo, YS, Feng, GF, et al., *Methods of Mathematical Physics*. National Defense Industry, Peking (2013)